Numerical Heat Transfer, Part A, 46: 23–40, 2004

ISSN: 1040-7782 print/1521-0634 online
DOI: 10.1080/10407780490457365

Taylor & Francis
Taylor & Francis Group

ULTRAFAST RADIATION HEAT TRANSFER IN LASER TISSUE WELDING AND SOLDERING

Kyunghan Kim and Zhixiong Guo
Department of Mechanical and Aerospace Engineering, Rutgers, The State University of New Jersey, Piscataway, New Jersey, USA

Laser tissue welding and soldering with use of short laser pulses are proposed. The transient radiation heat transfer in the picosecond time scale is numerically investigated for the first time using the discrete ordinate method for cylindrical geometries. The numerical method developed incorporates the propagation of radiation with the speed of light. The temporal radiation fields of tissue cylinders under the irradiation of short laser pulses are obtained. The use of short laser pulses for tissue welding and soldering is found to have reduced thermal damage to the healthy tissue and improves the uniformity of heating in the tissue closure region in both the depth and radial directions. The addition of absorbing solders in tissue soldering results in a well-confined radiation energy deposition field in the proximity of the solder-stained region and lessens the outgoing radiative heat flux at the laser incident surface. Comparisons of radiation heat transfer are made between the spatially square-variance and Gaussian-variance laser inputs and between the temporally Gaussian-profile and skewed-profile pulses, respectively.

1. INTRODUCTION

The study of short-pulsed laser radiation transport and ultrafast matter–radiation interactions is of great scientific and technological significance and is attracting increasing attention in recent years. Ultrafast radiation transfer is usually accompanied by the use of short-pulsed lasers. Ultrafast lasers with pulse width in the range from picoseconds down to femtoseconds can be used in a wide spectrum of emerging technologies, such as in optical tomography [1, 2], laser ablation [3, 4], laser material processing of microstructures [5, 6], and nanophotonics and nanotechnology [7–9], to name a few. Due to the very short time duration of the radiation–matter interaction and transport processes, many new phenomena occur. For example, our previous studies [10–12] have shown that inclusion of the time derivative term in the equation of radiation transfer (ERT) brings many new features. Here the concept of ultrafast radiation transfer is introduced in order to

Received 23 July 2003; accepted 30 January 2004.
Z. Guo acknowledges partial support of this research by the New Jersey Space Grant Consortium, National Science Foundation Grant CTS-0318001, the Charles and Johanna Busch Memorial Fund managed at Rutgers University, and an Academic Excellence Fund Award from Rutgers University.
Address correspondence to Zhixiong Guo, 98 Brett Road, Piscataway, NJ 08854, USA. E-mail: guo@jove.rutgers.edu

NOMENCLATURE

c	speed of light
D	diameter
H	depth
I	radiation intensity
M	number of angular discretization
n	refractive index
$\mathbf{r}$	position vector
R	radial direction
S	source term
t	time
t_p	pulse width
V	volume
w	angular weight
Z	axial direction
θ	azimuthal angle
μ, η, ξ	directional cosines
ρ	reflectivity
σ_a	absorption coefficient
σ_e	extinction coefficient
σ_s	scattering coefficient
ϕ	circumferential angle
ω	scattering albedo

Subscripts

b	blackbody value
d	downstream
p	control volume index
u	upstream
w	wall

Superscripts

d	diffuse
l	discrete direction index
s	specular

differentiate it from conventional transient radiation transfer in that only the time dependence of boundary conditions is considered, but the ERT is still stationary. In ultrafast radiation transfer, the governing equation is time-dependent and radiation propagates with the speed of light that is ultrafast. We have found that, when the pulse width of an incident laser is less than or comparable to the order of the characteristic time scale for radiation propagation defined by $t_c = L_c/c$ (L_c is the characteristic length), the ultrafast radiation transfer phenomenon occurs.

Solutions of the transient ERT in one-dimensional geometry for the case of short-pulse laser incidence have been reported in the literature [11, 13, 14]. Approaches that have extended to two-dimensional geometries include the first-order spherical harmonic (P_1) approximation [15], the discrete ordinate method [12], and the integral formulation [16]. However, the P_1 model underestimates the speed of light propagation [14] and the integral approach is difficult to apply to complex geometries. Recently, we have extended the discrete ordinate method to three-dimensional geometries in the Cartesian coordinate system [17, 18]. Monte Carlo simulation and experimental work have also been conducted [19]. There exists no published numerical method for ultrafast laser radiation transfer for curvilinear geometric problems.

The objective of the present investigation is twofold: (1) to develop the discrete ordinate method (DOM) for ultrafast radiation transfer in the cylindrical coordinate system; and (2) to study the characteristics of transient radiation heat transfer in tissue welding and soldering with the use of ultrafast lasers. The DOM for solving the steady-state ERT for cylindrical geometries is available in the literature [20, 21].

Laser welding of tissues is a surgical technique for bonding of tissues by using a laser beam to activate photothermal bonds and/or photochemical bonds. This method is potentially more advantageous than the conventional suturing technique because it is a noncontact method, which does not introduce foreign materials, and it is capable of forming an immediate watertight seal. For over 25 years, laser tissue welding has been studied as an alternative tool for tissue closure [22]. Typical tissue

closure methods include sutures, clips, or staples. Sutures create a scar during passage of the needle and tying the knot. This tissue scar and foreign body reaction can lead to inflammation, stenosis, and granuloma formation [23]. Unlike handcrafted sutures, clips and staples have limited range of adaptability in the face of different conditions such as tissue friability and thickness. Furthermore, these traditional methods are hardly applicable to tissue closure in microsurgery such as vascular anastomosis, closure of nerves, and uterine horn.

Laser tissue welding can be augmented with the use of solders. The solders can include chromophores that are used to control the laser penetration such that it is concentrated at the fusion site. Since extrinsic chromophores are not limited to the absorption characteristics of native tissue or body fluids, the solders may be tailored to selectively absorb energy that passes through normal tissue. The solders can also include other biochemical constituents to improve the weld strength and/or weld leakage characteristics. Typical additives include native collagen, gelatinous collagen, fibrin, elastin, and albumin.

Suitable lasers deliver wavelengths that are highly absorbed either by water or by the tissue's natural chromophores [24]. For example, argon lasers (488 and 514 nm) and KTP lasers (532 nm) are used with hemoglobin [25], Nd:YAG (1.064 and 1.320 μm) and CO_2 (10.6 μm) lasers are used with water [26]. Endogenous and exogenous materials such as indocyanine green (ICG) are often added to solders to enhance light absorption. ICG dye has a maximum absorption coefficient at 805 nm. Independent of the choice of chromophore, more energy is generally absorbed near the upper portion of the solder, closer to the laser spot. A temperature gradient is established over the depth of the solder. Depending on the temperature gradient and the laser exposure, the upper portion of the solder can become overcoagulated, while the most critical region, the solder/tissue interface, does not get fully coagulated. Such undercoagulated solder has been shown to create unstable bonds with tissue [27]. Hence, the clinical use of laser welding and soldering has been hindered [22] because of unreliable fusion strength, excessive thermal damage of tissue, nonuniform heating, etc.

Here we propose a new method for laser welding and/or soldering with short laser pulses as the irradiation source. When short laser pulses are used, the thermal diffusion to surrounding healthy tissues may be negligible and the thermal affected region is expected to be focused on the cutting and/or solder region. The possible advantages associated with the use of ultrafast lasers are the reduction of thermal damage, the improvement of heating uniformity, etc. A literature survey shows that such a study is novel.

In this article, we focus on the development of the discrete ordinate method for solving the ultrafast radiation heat transfer in cylindrical geometries. We use the numerical method developed to investigate the characteristics of time-dependent radiation heat transfer in ultrafast laser tissue welding and/or soldering.

2. MATHEMATICAL MODEL

Consider a collimated short laser pulse incident upon a biological tissue cylinder as shown in Figure 1. The ultrafast radiation heat transfer is described by the time-dependent ERT in the cylindrical coordinate system as

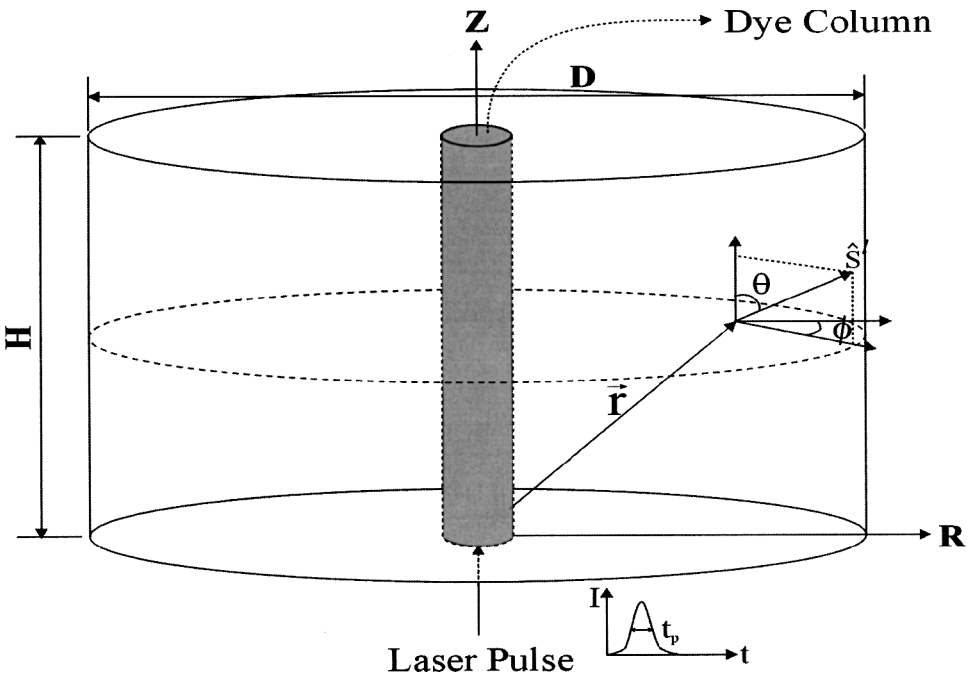

Figure 1. Geometric and coordinate sketches of laser welding and soldering in a tissue cylinder.

$$\frac{1}{c}\frac{\partial I^l}{\partial t}+\frac{\mu^l}{R}\frac{\partial}{\partial R}[RI^l]-\frac{1}{R}\frac{\partial}{\partial \phi}[\eta^l I^l]+\xi^l\frac{\partial I^l}{\partial Z}+\sigma_e I^l=\sigma_e S^l \qquad l=1,2,\ldots,M \tag{1}$$

where μ, η, and ξ are the three directional cosines for the discrete direction $\hat{s}^l$ (the superscript l is the index of discrete directions), I is the radiation intensity, σ_e is the extinction coefficient that is the sum of the absorption coefficient σ_a and the scattering coefficient σ_s, c is the speed of light in tissue, t is the time, and S^l is the source term that consists of three components:

$$S^l=(1-\omega)I_b^l+\frac{\omega}{4\pi}\sum_{i=1}^{M}w^i\Phi^{il}I^i+S_c^l \qquad l=1,2,\ldots,M \tag{2}$$

The first term on the right-hand side in Eq. (2) accounts for the blackbody emission of the tissue with human body temperature. The second term is the "in-scattering" contribution, in which, $\omega=\sigma_s/\sigma_e$ is the scattering albedo, $\Phi(\hat{s}^I\rightarrow\hat{s}^l)$ is the scattering phase function, and w^i $(i=1,2,\ldots,M)$ is the appropriate angular weight in the discrete direction $\hat{s}^i$. The last term in Eq. (2) is the external laser irradiation and can be expressed as

$$S_c^l=\frac{\omega}{4\pi}I_c(\mu^c\mu^l+\eta^c\eta^l+\xi^c\xi^l) \tag{3}$$

where the unit vector of (μ^c,η^c,ξ^c) represents the collimated laser incident direction.

For a pulse input that has a Gaussian profile in both spatial and temporal domains, the collimated laser radiation intensity at any location and time can be expressed as

$$I_c(R,Z,t) = I_0 \exp\left\{-4\ln 2 \times \left[\frac{(t-Z/c)}{(t_p-2)}\right]^2\right\} \times \exp\left(-\frac{R^2}{v^2}\right) \times \exp(-\sigma_e Z) \qquad (4)$$

In which t_p is the pulse width that is the full width at half-maximum (FWHM), $v^2/2$ is the spatial variance of the Gaussian incident beam, and I_0 is the maximum laser incident intensity. For a skewed-profile pulse in the temporal domain, it is composed of two different Gaussian profiles:

$$I_c(R,Z,t) = I_0 \exp\left\{-4\ln 2 \times \left[\frac{(t-Z/c)}{(t_p-2)}\right]^2\right\} \times \exp(-R^2/v^2) \times \exp(-\sigma_e Z) \qquad \text{for} \quad t \le t_p \qquad (5a)$$

$$I_c(R,Z,t) = I_0 \exp\left\{-4\ln 2 \times \left[\frac{(t-Z/c)}{(2t_p-2/3)}\right]^2\right\} \times \exp\left(-\frac{R^2}{v^2}\right) \times \exp(-\sigma_e Z) \qquad \text{for} \quad t > t_p \qquad (5b)$$

The laser intensity in the skewed pulse increases steeply until $t = t_p$ and then decreases gradually. So, this profile is skewed to the left side. In this research, we specify $I_0 = 0.46$ and consider a pulse duration from $t = 0$ to $4t_p$. In most of the present calculations we basically used a spatially square-variance pulse input, in which the intensity is uniformly spread over the laser beam.

In ultrafast laser radiation heat transfer, the blackbody emission of the participating medium is negligible. Such neglect does not introduce any appreciable error because: (1) the monochromatic laser intensity is much stronger than the blackbody emission of the medium; and (2) the laser pulse is extremely short, such that the thermal diffusion and temperature change in a short time are negligible.

There are two types of radiation boundary conditions in laser tissue welding or soldering. The first type is the tissue–air interface. The second type is the interface between healthy tissue and welding zone tissue. Specifically for Figure 1, all surfaces except the laser incident one are considered as the second type of boundary, in which the reflection of radiation is diffuse. Since biological tissues are highly scattering, laser radiation photons reaching these second-type boundaries have undergone multiple scattering events and the possibilities of photons passing through the boundary or reflecting back are equal. Thus, we specify a diffuse reflectivity of 0.5 at the second-type boundaries.

At the first-type interface, Fresnel reflection must be considered because of the mismatch of refractive indices between the tissue and air. This interface reflects and

refracts incident radiation. The refraction and reflection obey Snell's law and the Fresnel equation, respectively. Because the refractive index of tissue is greater than that of air, total reflection occurs when the incident angle θ_i of an internal radiation is not less than the critical angle $\theta_{cr} = \sin^{-1}(n_{air}/n_{Tissue})$. When $\theta_i < \theta_{cr}$, the reflectivity is calculated by the Fresnel equation:

$$\rho^s = \frac{1}{2}\left[\frac{\tan^2(\theta_i - \theta_r)}{\tan^2(\theta_i + \theta_r)} + \frac{\sin^2(\theta_i - \theta_r)}{\sin^2(\theta_i + \theta_r)}\right] \tag{6}$$

where θ_r is the refraction angle predicted by Snell's law. Under Fresnel boundary condition, the reflection is specular and the specular intensity is

$$I_w^l = (1 - \rho_w^{sl})I_{bw} + \rho_w^{sl} I^{-l} \tag{7}$$

For diffusely reflecting boundaries (at $R = D/2$ or $Z = H$), the boundary radiation intensity (e.g., at $Z = H$) is

$$I_w = (1 - \rho_w^d)I_{bw} + \frac{\rho_w^d}{\pi}\sum_{\xi^l<0}^{M/2} w^l I^l \left|\xi^l\right| \tag{8}$$

where ρ_w^d is the diffuse reflectivity of the surface. No real surface exists at $R = D/2$. There are surrounding healthy tissues beyond that surface and radiation heat transfer there is negligible because we mainly care about the heat transfer in the proximity of tissue closure region.

Along the centerline (at $R = 0$) of the tissue cylinder, an axisymmetric condition is applied.

3. NUMERICAL SCHEME

The DOM in our approach follows the S_N approximation [28]. A quadrature set of $M = N(N+2)$ discrete ordinates is used for the S_N method. In the present study, we basically used an S_{10} scheme [29], and no difference exists in the selection of quadrature scheme between curvilinear and rectangular geometries.

To solve Eq. (1), the finite-volume approach [28] is employed. The tissue cylinder is divided into numerous finite volumes. The discretized form of Eq. (1) in a cylindrical finite volume is

$$\frac{V}{c\Delta t}(I_p^l - I_p^{l0}) + \left|\mu^l\right|(A_{Rd}I_{Rd}^l - A_{Ru}I_{Ru}^l) - (A_{Rd} - A_{Ru})\left(\frac{\alpha_{p+1/2}I_{p+1/2}^l - \alpha_{p-1/2}I_{p-1/2}^l}{w_p}\right)$$
$$+ \left|\xi^l\right|(B_{Zd}I_{Zd}^l - B_{Zu}I_{Zu}^l) = \sigma_{eP}V(-I_p^l + S_p^l) \tag{9}$$

in which a direct-differencing technique [30] was used for the angular direction and a relationship exists [20, 21]:

$$\alpha_{p+1/2} - \alpha_{p-1/2} = w_p\mu_p \tag{10}$$

The subscripts d, u, and p stand for downstream, upstream, and the finite-volume center, respectively. The diamond scheme is used to relate the up- and downstream intensities in a finite-volume cell. The final discretization equation for the cell intensity in a generalized form is

$$I_p^l = \frac{(1/c\Delta t)I_p^{l0} + \sigma_e S_p^l + (A/V)|\mu_p| I_{ru}^l + (|\beta_p|/V) I_{p-1/2}^l + (B/V)|\xi_p| I_{zu}^l}{(1/c\Delta t) + \sigma_e + (A/V)|\mu_p| + (|\beta_p|/V) + (B/V)|\xi_p|} \tag{11}$$

where

$$A = A_{Ru} + A_{Rd} = 2R_p \,\Delta\phi\, \Delta Z \tag{12a}$$

$$\beta_p = \frac{(A_{Ru} - A_{Rd})(\alpha_{p+1/2} + \alpha_{p+1/2})}{w_p} \tag{12b}$$

$$B = B_{Zu} + B_{Zd} = 2R_p \,\Delta R\, \Delta\phi \tag{12c}$$

$$V = R_p \,\Delta\phi\, \Delta R\, \Delta Z \tag{12d}$$

Here, Δt is the time step, ΔR and ΔZ are the spatial steps in the radial and axial directions, respectively, and $\Delta\phi$ is the step change in the angular direction.

Uniform grid sizes in time, space, and angle domains were adopted in the present calculations. The staggered (R, ϕ, Z) grid size was $42 \times 62 \times 22$ for a typical tissue cylinder with $D = 10$ mm and $H = 2$ mm. The time step for this typical tissue cylinder was $\Delta t = 0.5$ ps. We used a Dell PC with 512 MB of memory for the calculations. For an S_{10} numerical scheme, there are 120 ERTs to be solved simultaneously. Thus, we could not further refine the grid size because of computer memory limitation. However, the calculations were compared among several sets of grid size and the outcome was satisfactory.

In order to examine our numerical algorithm, we applied the transient DOM to solve a steady-state radiation heat transfer problem in a cylindrical furnace and compared our numerical results with the published experimental measurement. The cylindrical furnace, of diameter 0.90 m, is 5.1 m long. Its temperature field is given elsewhere [21]. The radiative heat flux at the furnace side wall was measured experimentally by Wu and Fricker [31]. Figure 2 shows the comparisons between the experimental measurement and our numerical predictions using the S_4 and S_{10} schemes. It is observed that the predicted wall heat flux profiles are consistent with the experimental data. In particular, the S_{10} result matches the measurement closely.

4. RESULTS AND DISCUSSION

Now the transient DOM in cylindrical coordinates is used to study radiation heat transfer in ultrafast laser tissue welding and/or soldering. The general dimensions of the tissue cylinder are $D = 10$ mm and $H = 2$ mm. The optical properties of the tissue are $\sigma_a = 0.001\,\text{mm}^{-1}$ and $\sigma_s = 1.00\,\text{mm}^{-1}$. Here the reduced scattering coefficient of general biological tissue is used. Thus, anisotropic scattering is reduced to isotropic scattering. However, the present algorithm can treat anisotropy of

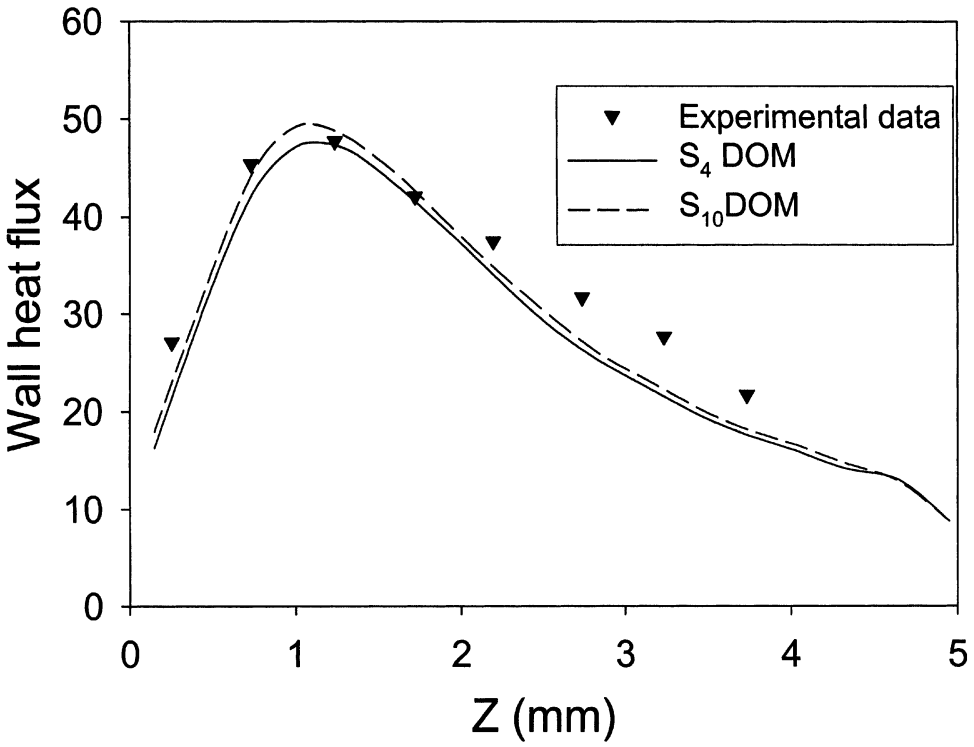

Figure 2. Comparison of surface radiative heat flux in an example cylindrical furnace between experimental measurement [31] and numerical predictions.

scattering. When laser soldering is involved, 6.5 μM ICG is spread uniformly in the dye column, which is 0.5 mm in diameter as shown in Figure 1. The absorption coefficient of the ICG dye solder is $\sigma_a = 0.17\,\text{mm}^{-1}$ [32]. We still assume $\sigma_s = 1.00\,\text{mm}^{-1}$ in the solder column. Uniform finite-volume meshes are adopted with $\Delta R = 0.125\,\text{mm}$, $\Delta Z = 0.1\,\text{mm}$, and $\Delta\phi = 6°$. The time resolution is $\Delta t = 0.5\,\text{ps}$. The refractive index of the biological tissue is assumed to be 1.4. A short laser pulse is normally incident from the center of the tissue surface at $Z = 0$. The beam diameter and pulse width of the incident laser are $d_c = 0.88$ mm and $t_p = 10$ ps, respectively.

Figure 3 compares the temporal profiles of the divergence of radiative heat flux at different axial locations along the centerline of the cylinder for both the laser welding (without use of dye) and the laser soldering (with use of the ICG dye). The divergence of radiative heat flux represents the absorbed or deposited volumetric laser energy in the medium. The incident laser pulse was spatially flat, i.e., square-variance over the beam diameter. Three axial locations were selected, at the laser incident spot ($Z/H = 0$), at the midplane of the tissue ($Z/H = 0.5$), and at the exit of the laser pulse ($Z/H = 1.0$). At any location, the absorbed radiation energy is found to increase rapidly to the maximum value with the input of a short laser pulse and then to decrease exponentially. Initially there is a very intense energy deposition at the location close to the laser incident spot ($Z/H = 0$). For $t > 4t_p = 40$ ps, the radiation energy deposition is even lower in the proximity of the laser incident spot

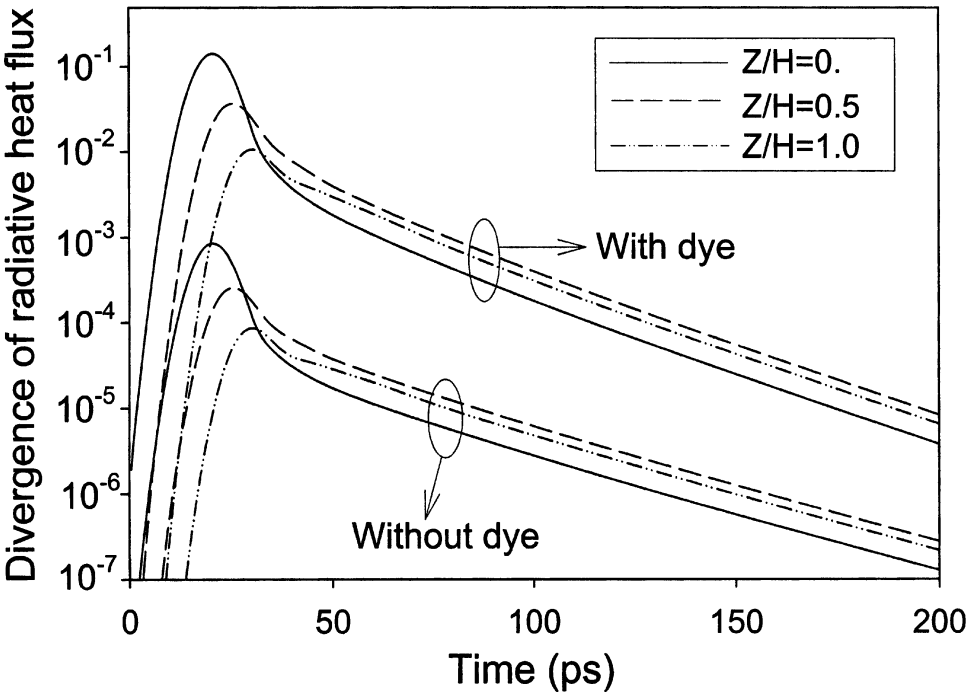

Figure 3. Temporal profiles of the divergence of radiative heat flux at three locations in the cylindrical centerline for both the laser tissue welding and soldering.

than at other axial locations because the irradiation of incident pulse ends at $4t_p$. This is different from continuous wave (CW) laser welding or soldering, in which the radiation energy deposition in the proximity of the incident spot is always the strongest. This unique feature of the proposed ultrafast laser tissue welding and soldering is of great significance because it suggests that overcoagulation in the closure tissue surface owing to larger energy deposition in the proximity of the laser spot can be avoided.

The temporal variations under the welding condition in Figure 3 are very similar to those under the soldering condition except for the magnitude of the values of the divergence of radiative heat flux. The radiation energy deposition is almost two orders of magnitude larger in the laser soldering than in the laser welding. This is because of the addition of relatively strongly absorbing dye in the fusion region in the laser soldering.

Figure 4 shows the profiles of the net outgoing radiative heat flux along the laser–tissue interface at different time instants. Comparison is made between the laser welding and soldering. The use of solder diminishes the outgoing surface radiative heat flux because of the enhancement of laser energy absorption inside the fusion region. Particularly in the region (e.g., $R < 1$ mm) close to the solder-stained region ($R < 0.25$ mm), the reduction of outgoing surface heat flux is substantial. Also, it is noticed that the use of solder improves the uniformity of the radiative heat flux profile along the tissue–air surface. At the early time stage, the outgoing

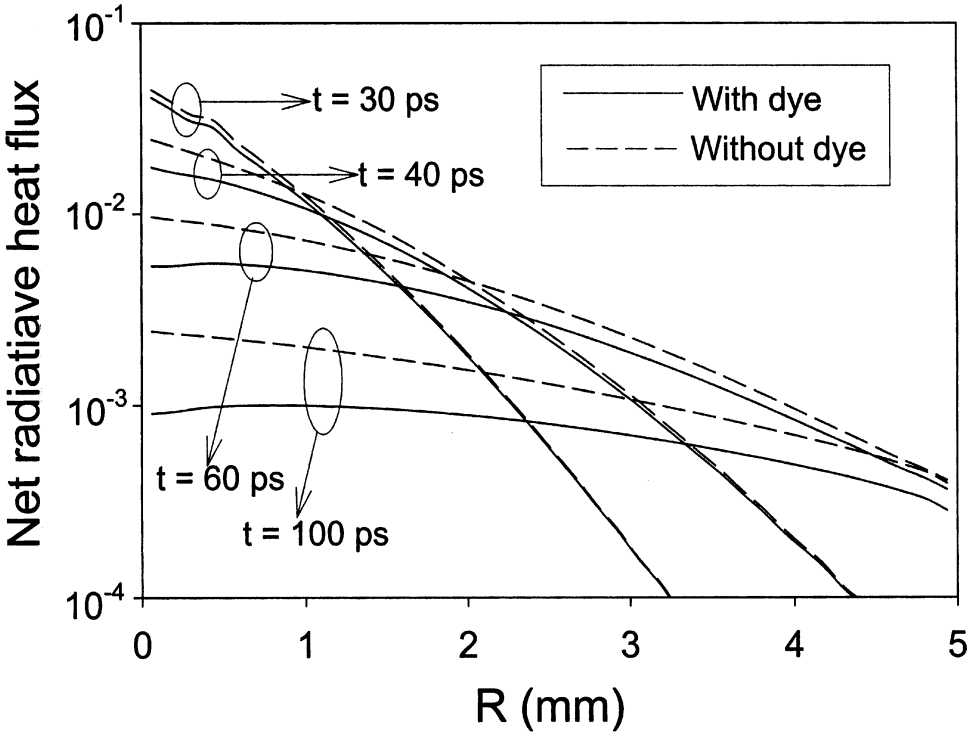

Figure 4. Comparison of radiative heat flux profiles on the laser incident surface between the laser welding and soldering for different time instants.

radiation is focused on the center of the surface (i.e., around $R=0$). With the advance of time, it is seen that the profiles of radiative heat flux become flatter. A flatter profile may help improve the formation of tissue closure scar. For CW laser welding or soldering, however, a steady gradient variation always exists in the profiles.

The profiles of the divergence of radiative heat flux along the centerline of the tissue cylinder are compared between the laser welding and soldering in Figure 5. As far as the relative shape of the energy absorption profile is concerned, no obvious difference is found between the results of the two different laser closure conditions. Again, the magnitude of the absolute value of the energy deposition is very different. The radiation energy absorption under the soldering condition is about two orders of magnitude larger than that under the welding condition. The profiles become flatter as time elapses. This may lead to uniform heating throughout the depth direction when short pulses are deployed for laser welding and soldering. It may improve the mechanical strength of the closure.

The contour plots of the divergence of radiative heat flux at the R–Z half-plane are displayed in Figures 6 and 7 (color figures are available at http://coewww.rutgers.edu/radiation/publications.html) for laser welding and soldering conditions, respectively. Six time instants ($t=20$, 30, 40, 50, 60, and 100 ps) were selected for comparison. As time advances, the radiation field propagates from the incident laser

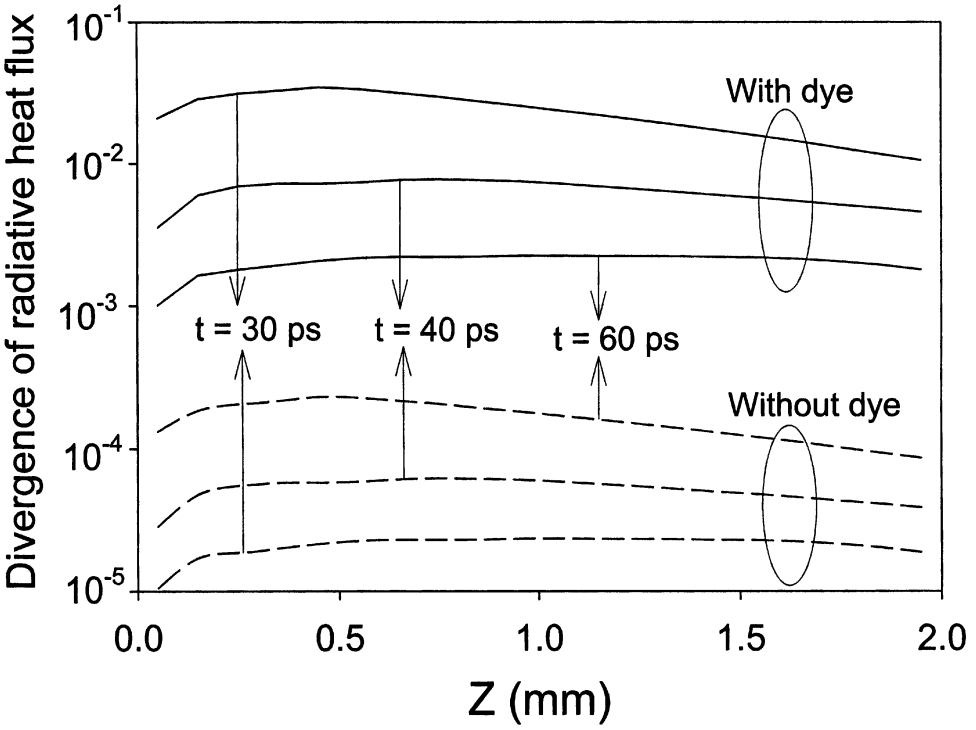

Figure 5. Profiles of the divergence of radiative heat flux along the centerline for various time instants for both the laser welding and soldering.

spot to most of the area of the cylinder. At the early time stages ($t < 50$ ps), the wave propagation phenomenon is very obvious. Such a phenomenon could not be visualized if the time derivative term in the ERT were neglected, nor could it be correctly predicted if a diffusion approximation that is commonly adopted in biomedical engineering field [2] were adopted. After $t > 50$ ps, the radiation transport gradually becomes diffused. A diffusion field clearly exists at $t = 100$ ps. The characteristic time scale for radiation propagation is $t_c = H/c \approx 10\,ps$ in the present study system, and the pulse width of the irradiation is also $t_p = 10\,ps$. In general, when t_p is less than or comparable to t_c, the time derivative term in the ERT (or, say, ultrafast radiation transfer) must be incorporated. After time reaches to $t = 10t_c$, the radiation propagates diffusely. These findings are consistent with our previous research [11, 19].

It is clear that the radiation field in Figure 6 under the laser welding condition is diffusing from the centerline to the surrounding tissue region with the advance of time, whereas the radiation field in Figure 7 under the laser soldering condition is well confined in the absorbing solder-sustained region. Thus, thermal damage to the surrounding healthy tissue is a concern in clinical laser tissue welding and it can be quantitatively justified using a radiation heat transfer model in conjunction with heat conduction. On the other hand, the very strong radiation energy deposition in the solder-stained region in the laser tissue soldering may cause overcoagulation in the

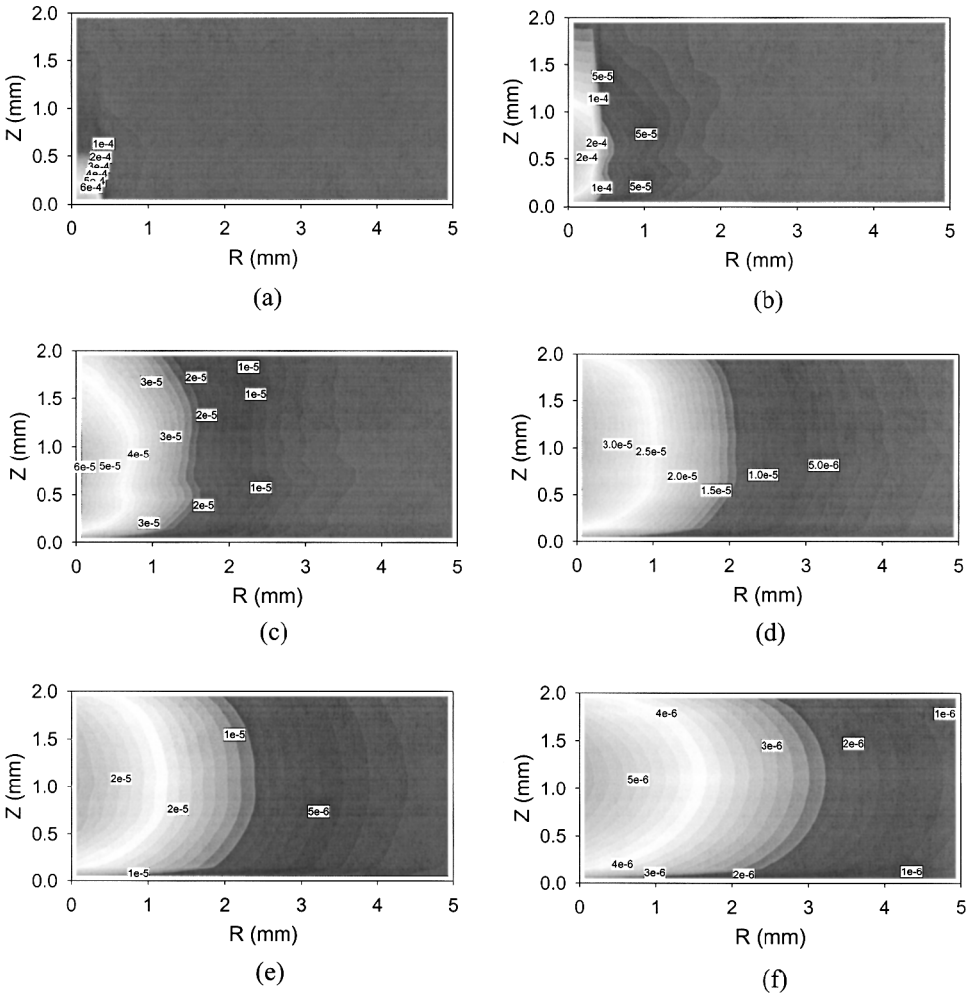

Figure 6. Contours of divergence of radiative heat flux at various time instants for laser welding: (*a*) $t = 20$ ps; (*b*) $t = 30$ ps; (*c*) $t = 40$ ps; (*d*) $t = 50$ ps; (*e*) $t = 60$ ps; (*f*) $t = 100$ ps.

lower portion of the solder that is close to the laser incident spot. However, it is seen from Figure 7 that the peak energy deposition is shifting to the upper portion of the solder with the increase of time. Such a feature is unique with ultrafast laser soldering, and it may lessen the overcoagulation phenomenon. A model-based optimal design of an ultrafast laser soldering system may make a breakthrough in laser tissue soldering technology and enable its clinical application. This will be our work in the near future. In Figure 7, the region at $R > 2$ mm has been cut in order to enhance the view of the radiation field in the solder-sustained region.

In the above laser tissue welding and soldering studies, spatially square-variance laser pulses were employed. To investigate the effect of the spatial variance of the laser beam, both square-variance and Gaussian-variance beams with a beam diameter of 0.88 mm are used as the irradiation source. The profiles of the diver-

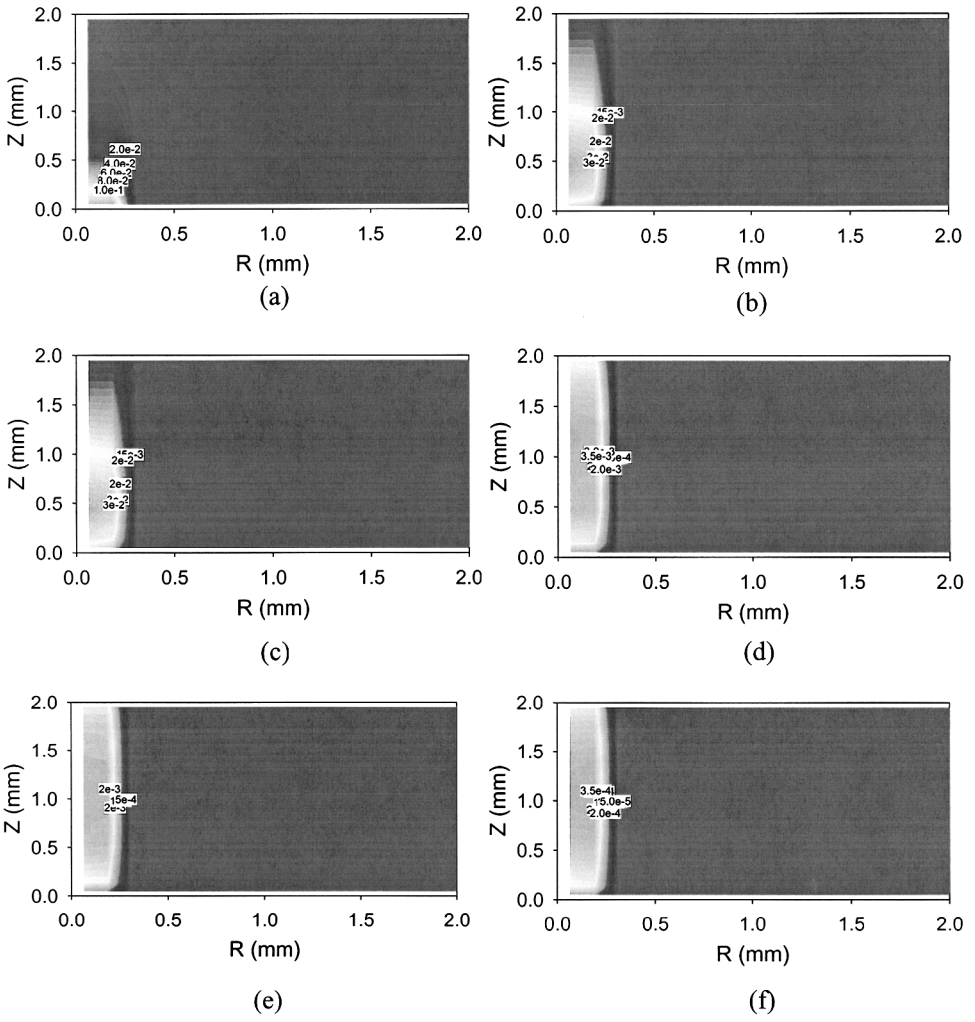

Figure 7. Contours of divergence of radiative heat flux at various time instants for laser soldering: (*a*) $t = 20$ ps; (*b*) $t = 30$ ps; (*c*) $t = 40$ ps; (*d*) $t = 50$ ps; (*e*) $t = 60$ ps; (*f*) $t = 100$ ps.

gence of radiative heat flux along the radial direction at a specified axial location ($Z/H = 0.5$) are compared between the square-variance beam and the Gaussian beam in Figure 8 under the laser welding condition. Although the incident radiation intensity is spatially uniform over the range of the beam under the spatially flat laser beam condition, there exists a gradient of the divergence of radiative heat flux along the radial direction. Of course, the gradient for the square-variance beam input is smaller than that for the Gaussian beam input. Clearly the square-variance beam can improve the uniform heating condition in the radial direction in laser tissue welding.

Figure 9 exhibits the temporal profiles of the divergences of radiative heat flux in tissue welding under the laser irradiations of temporally Gaussian and skewed pulses. Three different axial locations in the cylinder centerline are chosen for

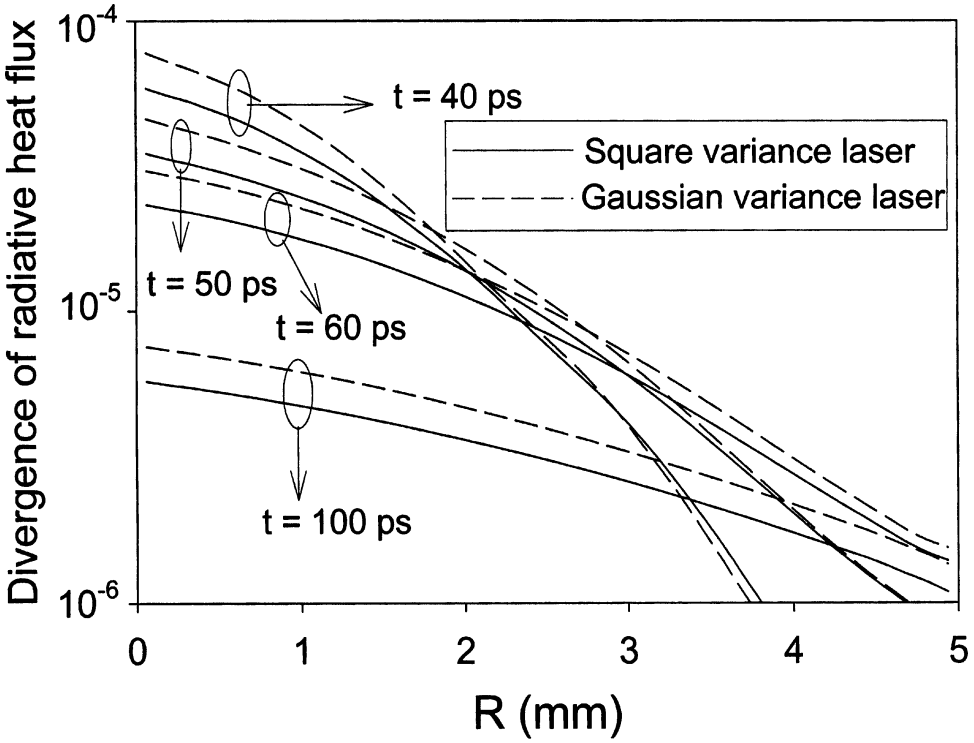

Figure 8. Influence of the spatial profile of incident laser pulse on the divergence of radiative heat flux along the radial direction at $Z/H = 0.5$ for laser welding.

comparison. Although the two pulses have the same pulse width ($t_p = 10$ ps) and the same time duration of irradiation (starts at $t = 0$ and ends at $4t_p$), the peak times of these two pulses are different. For the skewed-profile pulse the peak intensity is at $t = 10$ ps, while for the Gaussian-profile pulse it is at $t = 20$ ps. It is observed from Figure 9 that the radiation energy deposition rises faster for the skewed pulse than for the Gaussian pulse. The difference in response time is about 10 ps. Except for that, the temporal shapes of the absorbed radiation energy for these two input pulses are quite similar. A skewed pulse may describe the temporal profiles of incident laser pulses more realistically.

In the above calculations, we considered a 2-mm-thick tissue cylinder with a diameter of 10 mm. The value of tissue cylinder diameter was selected such that the radiation field region of interest would not be obviously affected by the cylinder wall boundary condition. The results in Figures 6 and 7 have shown that the radiation fields region of interest (e.g., $R < 3$ mm) within the time period of interest (e.g., $t < 100$ ps) is not influenced by the specific diameter value. The choice of cylinder depth value depends on specific tissue closure conditions. Figure 10 illustrates the profiles of the divergence of radiative heat flux along the centerline for tissue welding of different values of tissue thickness with $H = 2$, 4, and 6 mm. At $t = 30$ ps, the profiles for the three selected tissue depths nearly overlap. As time elapses, the

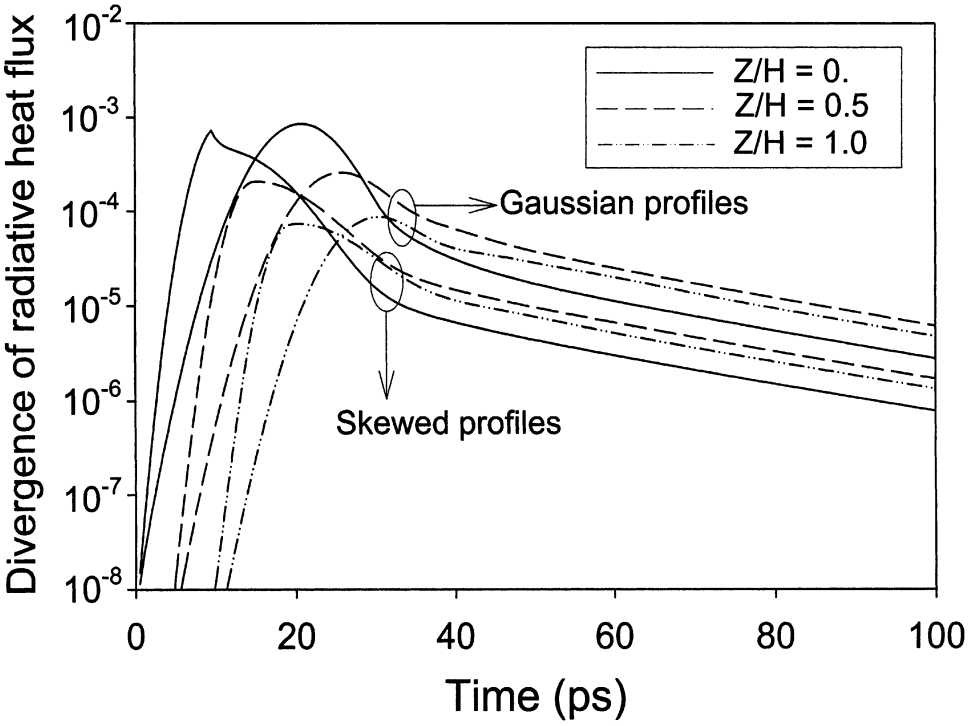

Figure 9. Comparison of temporal divergence of radiative heat flux at different axial locations in the centerline between the temporally Gaussian-profile pulse and the skewed-profile pulse.

difference becomes obvious, particularly at the laser exit end. However, it is still not very appreciable except for the case at $t = 100$ ps, where, however, the magnitude of the divergence of radiative heat flux is very small. For thicker tissue closure (e.g., $H = 6$ mm), a steep declination of the divergence of radiative heat flux exists at the laser exit end, and this may result in undercoagulation.

5. CONCLUSIONS

We proposed an ultrafast laser tissue welding and soldering method with the use of picosecond laser pulses as the irradiation source. The aim is to diminish the thermal diffusion and damage associated with conventional CW or relatively long-pulsed laser tissue welding and soldering. The discrete ordinate method for ultrafast radiation transfer in cylindrical geometries has been developed. The numerical method has been compared with the published experimental measurement in an example problem. The characteristics of ultrafast laser radiation heat transfer in tissue welding and soldering have been intensively investigated. The time-resolved as well as the spatially resolved radiation heat transfer information has been obtained. It has been found that the laser energy deposition in the proximity of the laser incident spot decreases rapidly immediately after the incidence of a short laser pulse.

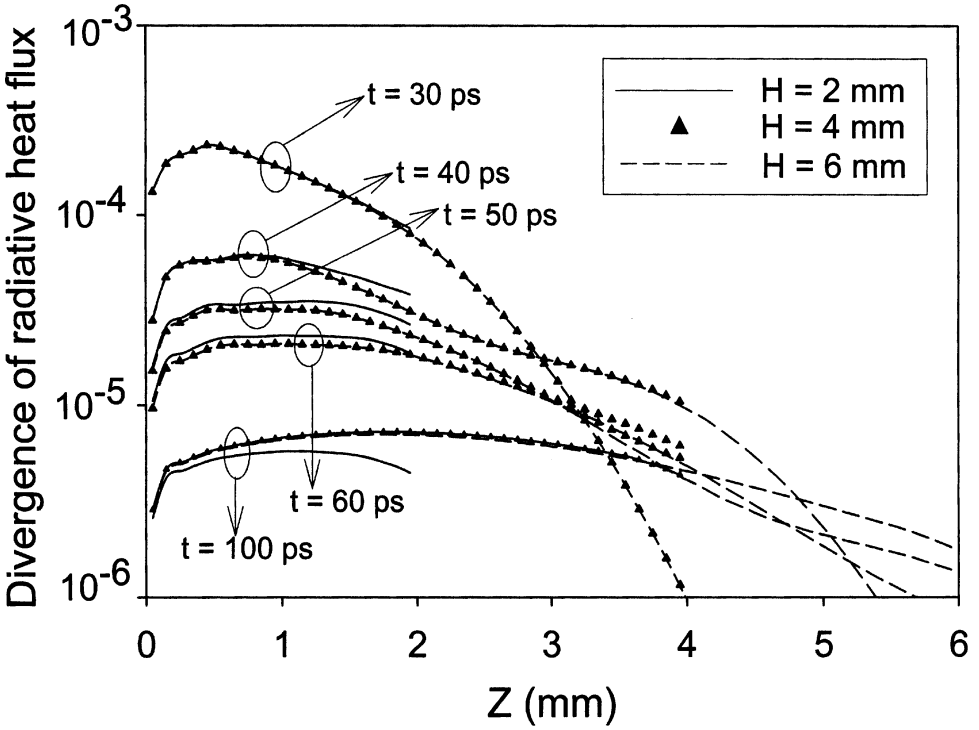

Figure 10. Profiles of divergence of radiative heat flux along the cylindrical centerline for different values of cylinder thickness in tissue welding.

This could avoid overcoagulation in the fusion region. The use of short pulses also results in flatter profiles of the divergence of radiative heat flux along the fusion depth direction and of the outgoing radiative heat flux along the radial direction on the tissue surface. These help improve the uniformity of heating and, consequently, may better the quality of the closure. These are unique features of ultrafast laser tissue welding and soldering. We also found that thermal radiation diffusion to surrounding healthy tissue occurs in the tissue welding processes at 50–100 ps ($= 5$–$10t_c$) after the incidence of the laser pulse, whereas the radiation field is well confined in a very narrow solder-stained region in the tissue soldering processes. The radiation field is always time-dependent and dynamic. As a result, no constant radiation gradient will be established inside the tissue, either in the radial direction or in the axial direction. The location of the peak radiation energy deposition is always moving. This makes it achievable to design an optimal laser tissue welding or soldering condition. For thicker tissue closure, it is more difficult to realize uniform heating condition along the fusion depth. The use of a spatially flat laser beam yields a relatively uniform heating outcome in the radial direction as compared with the use of a Gaussian beam input. The difference of radiation field between the temporally Gaussian-profile and skewed-profile pulses is not appreciable except for the radiation response time.

REFERENCES

1. S. Kumar, P.-F. Hsu, K. Mitra, B. Garetz, Z. Guo, and J. Aber, Radiative Transfer Modeling and Experiments Using Short Pulse Lasers, in K. P. Chong, S. Saigal, S. Thynell, and H. S. Morgan (Eds.), *Modeling and Simulation Based Life Cycle Engineering*, pp. 170–184, Spon Press, Taylor & Francis Group, New York, 2002.
2. Y. Yamada, Light–Tissue Interaction and Optical Imaging in Biomedicine, *Annu. Rev. Heat Transfer*, vol. 6, pp. 1–59, 1995.
3. F. H. Loesel, F. P Fisher, H. Suhan, and J. F. Bille, Non-thermal Ablation of Neural Tissue with Femtosecond Laser Pulses, *Appl. Phys. B.*, vol. 66, pp. 121–128, 1998.
4. V. V. Kancharla and S. C. Chen, Fabrication of Biodegradable Polymeric Micro-devices Using Laser Micromachining, *Biomed. Microdevices*, vol. 4, pp. 105–109, 2002.
5. J. P. Longtin and C. L. Tien, Microscale Radiation Phenomena, in C. L. Tien, A. Majumdar, and F. M. Gerner (Eds.), *Microscale Energy Transport*, pp. 119–147, Taylor & Francis, Washington, D.C. 1997.
6. C. P. Grigoropoulos, H. K. Park, and X. Xu, Modeling of Pulsed Laser Irradiation of Thin Silicon Layers, *Int. J. Heat Mass Transfer*, vol. 36, pp. 919–924, 1993.
7. A. Majumdar, Scanning Thermal Microscopy, *Annu. Rev. Mater. Sci.*, vol. 29, pp. 505–585, 1999.
8. X. Wang and X. Xu, Thermoelastic Waves Induced by Pulsed Laser Heating, *Appl. Phys. A*, vol. 73, pp. 107–114, 2000.
9. Y. Shen, C. S. Friend, Y. Jiang, D. Jakubczyk, J. Swiatkiewicz, and P. N. Prasad, Nanophotonics: Interactions, Materials, and Applications, *J. Phys. Chem. B*, vol. 140, pp. 7577–7877, 2000.
10. Z. Guo, S. Kumar, and K.-C. San, Multi-dimensional Monte Carlo Simulation of Short Pulse Laser Radiation Transport in Scattering Media, *J. Thermophys. Heat Transfer*, vol. 14, pp. 504–511, 2000.
11. Z. Guo and S. Kumar, Radiation Element Method for Transient Hyperbolic Radiative Transfer in Plane-Parallel Inhomogeneous Media, *Numer. Heat Transfer B*, vol. 39, pp. 371–387, 2001.
12. Z. Guo and S. Kumar, Discrete-Ordinates Solution of Short-Pulsed Laser Transport in Two-Dimensional Turbid Media, *Appl. Opt.*, vol. 40, pp. 3156–3163, 2001.
13. S. Kumar, K. Mitra, and Y. Yamada, Hyperbolic Damped-Wave Models for Transient Light-Pulse Propagation in Scattering Media, *Appl. Opt.*, vol. 35, pp. 3372–3378, 1996.
14. K. Mitra and S. Kumar, Development and Comparison of Models for Light Pulse Transport through Scattering Absorbing Media, *Appl. Opt.*, vol. 38, pp. 188–196, 1999.
15. K. Mitra, M. S. Lai, and S. Kumar, Transient Radiation Transport in Participating Media within a Rectangular Enclosure, *J. Thermophys. Heat Transfer*, vol. 11, pp. 409–414, 1997.
16. Z. M. Tan and P. Hsu, An Integral Formulation of Transient Radiative Transfer, *J. Heat Transfer*, vol. 123, pp. 466–475, 2001.
17. Z. Guo and S. Kumar, Three-Dimensional Discrete Ordinates Method in Transient Radiative Transfer, *J. Thermophys. Heat Transfer*, vol. 16, pp. 289–296, 2002.
18. Z. Guo and K. H. Kim, Ultrafast-Laser-Radiation Transfer in Heterogeneous Tissues with the Discrete-Ordinates Method, *Appl. Opt.*, vol. 42, pp. 2897–2905, 2003.
19. Z. Guo, J. Aber, B. Garetz, and S. Kumar, Monte Carlo Simulation and Experiments of Pulsed Radiative Transfer, *J. Quant. Spectrosc. Radiative Transfer*, vol. 73, pp. 159–168, 2002.
20. J. R. Tasi and N. Ozisik, Radiation in Cylindrical Symmetry with Anisotropic Scattering and Variable Properties, *J. Heat Mass Transfer*, vol. 33, pp. 2651–2658, 1990.
21. A. S. Jamaluddin and P. J. Smith, Predicting Radiative Transfer in Axisymmetirc Cylindrical Enclosures Using the Discrete Ordinates Method, *Combustion Sci. Technol.*, vol. 62, pp. 173–186, 1988.

22. N. M. Fried, V. C. Hung, and J. T. Walsh, Laser Tissue Welding: Laser Spot Size and Beam Profile Studies, *IEEE J. Quantum Electron*., vol. 5, pp. 1004–1012, 1999.
23. L. S. Bass and M. R. Treat, Laser Tissue Welding: A Comprehensive Review of Current and Future Applications, *Lasers Surg. Med*., vol. 17, pp. 315–349, 1995.
24. D. P. Poppas, G. B. Rucker, and D. S. Scherr, Laser Tissue Welding—Poised for the New Millenium, *Surg. Technol. Int*., vol. IX, pp. 33–41, 2000.
25. L. W. Murray, L. Su, G. E. White, and R. A. White, Cross Linking of Extracellular Matrix Proteins: A Preliminary Report on a Possible Mechanism of Argon Laser Welding, *Lasers Surg. Med*., vol. 9, pp. 490–496, 1989.
26. R. P. Abergel, R. Lyons, R. Dwyer, R. A. White, and J. Uitto, Use of Lasers for Closure of Cutaneous Wounds: Experience with Nd:YAG, Argon, CO_2 Lasers, *J. Dermatol. Surg. Oncol*., vol. 12, pp. 1181–1185, 1986.
27. K. M. McNally, B. S. Song, E. K. Chan, A. J. Welch, J. M. Dawes, and E. R. Owen, Optimal Parameters for Laser Tissue Soldering. Part I: Tensile Strength and Scanning Electron Microscopy Analysis, *Lasers Surg. Med*., vol. 24, pp. 319–331, 1999.
28. M. F. Modest, *Radiative Heat Transfer*, chap. 15, McGraw-Hill, New York, 1993.
29. W. A. Fiveland, The Selection of Discrete Ordinate Quadrature Sets for Anisotropic Scattering, ASME HTD, Fund. of Rad. Heat Transfer; Vol. 72, pp. 89–96, 1991.
30. B. G. Carson and K. D. Lathrop, Transport Theory—The Method of Discrete Ordinates, in H. Greenspan, C. N. Kelber, and D. Okrent (Eds.), *Computing Methods in Reactor Physics*, Gordon & Breach, New York, 1968.
31. H. L. Wu and N. Fricker, An Investigation of the Behavior of Swirling Jet Flames in a Narrow Cylinder Furnace, The 2nd Members' Conference, International Flame Research Foundation, Ijmuiden, The Netherlands, 1971.
32. M. L. J. Landsman, G. Kwant, and G. A. Mook, and W. G. Zijlstra, Light-Absorbing Properties, Stability, and Spectral Stabilization of Indocyanine Green, *J. Appl. Physiol*., vol. 40, pp. 575–583, 1976.